Materials Science and Engineering A 523 (2009) 70–76

Contents lists available at ScienceDirect

Materials Science and Engineering A

journal homepage: www.elsevier.com/locate/msea

Porous NiTi by creep expansion of argon-filled pores

Scott M. Oppenheimer[1], David C. Dunand*

Department of Materials Science and Engineering, Northwestern University, Evanston, IL, 60208-3108, USA

ARTICLE INFO

Article history:
Received 23 March 2009
Received in revised form 15 May 2009
Accepted 20 May 2009

Keywords:
Cellular materials
Metallic foams
Nitinol
Hot isostatic pressing
Powder metallurgy
Stiffness
Microstructure

ABSTRACT

NiTi powders are densified in the presence of argon gas, whose initial pressure is varied between 1 and 33 atm, to create NiTi billets containing isolated Ar-filled pores. Upon vacuum annealing, the pressurized pores expand by creep of the surrounding NiTi matrix at rates which are in agreement with a simple analytical model up to 16% porosity. Beyond this porosity, foaming becomes very slow, as pores connect with each other and with the specimen surface where the gas escapes. This is due to failure of previous NiTi powder boundaries weakened by oxides insoluble in NiTi; this mechanism does not occur in Ti foams which dissolve their oxides at high temperature, allowing higher levels of pore expansion and foam porosity. NiTi with 10–16% porosity exhibits Young's moduli of 48–57 GPa, and may be useful for high-strength, low stiffness biomedical implants with superelastic or shape-memory properties.

1. Introduction

Near-equiatomic nickel–titanium alloys (NiTi) are used for various medical devices due to their excellent biocompatibility [1,2] high strength and toughness, and their superelastic or shape memory properties [3]. While NiTi is the least stiff among the main biocompatible alloys (steel, Co- or Ti-based alloys), it is much stiffer than bone, leading to stress-shielding between implant and bone and eventual implant failure. As recently reviewed [4], porous NiTi created by a variety of methods can exhibit very low stiffness matching that of bone, while also showing open porosity allowing bone ingrowth [5–12,26]. Foam fabrication methods based on the reaction of elemental powders have the advantages of rapid processing and low powder costs, but offer limited control over the pore fraction and architecture, and may result in undesirable off-stoichiometric phases. By contrast, methods based on sintering of prealloyed NiTi powders allow better control of porosity and composition, but they suffer from the high cost, low sinterability of NiTi powders, and their propensity for creating stable oxides layers.

The low sinterability of prealloyed NiTi powders [10] can be addressed by using a solid-state foaming process, first demonstrated for Ti–6Al–4V by Kearns et al. [13] and recently extended to NiTi by Greiner et al. [14]. In this method, metallic powders are placed in a steel can which is evacuated and then backfilled with argon. The sealed can is then densified in a hot isostatic press (HIP) at high temperature and pressure, resulting in a nearly dense metallic billet containing small, isolated pores filled with argon. After removing the steel can, the billet is exposed to high temperatures under vacuum to allow the expansion of the pressurized pores by creep of the surrounding metallic matrix. Greiner et al. [14] found that NiTi foamed very rapidly by this method at 1200 °C, i.e. reaching ~11% porosity in less than 1 h; this was followed by a much slower porosity increase to ~19% porosity (4–8 days). The resulting porous NiTi exhibited superelastic behavior, a high compressive strength and a Young's modulus of 41 GPa, as measured ultrasonically. The apparent stiffness, as measured from stress–strain curves, could be altered by heat-treatment and reached values as low as 14 GPa.

In the present paper, we study solid-state foaming of NiTi in more detail by varying the foaming temperature and the amount of trapped argon, and by modeling the expansion process. We also elucidate the reason for the abrupt change of foaming rate observed to occur at ~11% porosity by Greiner et al. [14] and the low terminal porosities achieved with NiTi foams, as compared to Ti or Ti–6Al–4V foams processed by the same method [13,15,16]. Finally, we measure the stiffness of porous NiTi ultrasonically.

2. Experimental procedures

2.1. Powder densification

Prealloyed martensitic NiTi powders (49.4 at.% Ni, 99.9% purity, 44–177 μm size, from Specialty Metals Corp., NY) were mixed for

* Corresponding author. Tel.: +1 847 491 5370.
E-mail address: dunand@northwestern.edu (D.C. Dunand).
[1] Present address: ATI Allvac, 2020 Ashcraft Ave, Monroe, NC 28111-5030, USA.

0921-5093/$ – see front matter © 2009 Elsevier B.V. All rights reserved.
doi:10.1016/j.msea.2009.05.045

at least 1 h with small quantities of elemental nickel powders (99.9% purity, 44–177 μm size, from Specialty Metals Corp., NY) to increase the Ni/Ti ratio. A first group of billets, initially described by Greiner et al. [14] and labeled A and B in Table 1, had been canned and backfilled with Ar by the HIP company (UltraClad, Andover, MA) in 35.0 mm diameter cans with a 1.6 mm wall thickness, using pre-mixed powders with an average Ni composition of 51.0 at.%. A second group of cans, labeled 1–8 in Table 1, was filled for the present study with mixed powders with 50.2% Ni average composition, Ar-backfilled and sealed in our laboratory, and sent to UltraClad for densification. Densification occurred at 1066 °C for 4 h at a pressure of 1020 atm (103 MPa) for billets A and B, and 1800 atm (152 MPa) for billets 1–8. While the small change in composition from 50.2 to 51 at.% affects the room temperature mechanical properties of the foams (in particular their shape-memory and superelastic behavior), it is inconsequential for their creep properties [17] which control the foaming kinetics.

For billets 1–8 prepared in our laboratories, the powders were poured and packed by hand with a steel rod into a low-carbon steel tube (7.04 and 9.53 mm inner and outer diameter and ~50 cm length) with a crimped and welded bottom. After multiple flushings with Ar, the tube was backfilled with 99.999% pure Ar and crimp-welded. This method was used up to 5 atm Ar, above which the pressurized gas burst through the weld area during the sealing process. A new method was developed to increase the Ar content above that limit. The welded lower end of the long tubes was immersed in liquid nitrogen (77 K boiling point [18]) which led to condensation of solid Ar (84 K freezing point [18]) within the tube. Very large quantities of solid Ar could be trapped in the tube while keeping a low Ar pressure (equal to its vapor pressure at 77 K) allowing easy weld-sealing of the can. The Ar amount introduced in the tube was metered, from which the gas pressure, after the sealed tube has returned to ambient temperature, was calculated, as reported in Table 1.

Because of the somewhat irregular shape of the tubes after HIP consolidation, the steel can was removed electro-chemically rather than by turning. The process occurred under a 2 V voltage in an aqueous 10% acetic acid solution with NaCl. The less noble steel can was dissolved preferentially, while the nobler NiTi billet was cathodically protected. The NiTi billet was then sanded to remove a thin surface layer contaminated by reaction with steel during HIP and oxidized during the steel removal, and finally sectioned on a diamond saw into cylindrical test specimens 15–20 mm in height and ~6 mm in diameter. For the larger HIP consolidated billets A and B, samples were cut by electro-discharge machining (EDM) into 6 mm cubes whose sides were polished with 400 grit SiC paper to remove the damaged layer.

2.2. Solid-state foaming

Foaming was performed at 900 or 1150 °C in a high-vacuum furnace (residual pressure $<10^{-5}$ Torr, typically $\sim 4 \times 10^{-6}$ Torr, measured at the chamber) with molybdenum heating elements. Samples were placed on a boron-nitride-coated molybdenum mesh and surrounded by a titanium tube (25.4 mm outer diameter, 100 mm high) acting as a getter. Temperature was measured outside the tube with a K-type thermocouple coated with boron nitride. Tests with a second thermocouple confirmed that no measurable temperature difference existed between the inside and outside of the tube. At regular intervals during foaming, the sample was cooled to ambient temperature and its density was measured by the Archimedes method in deionized water, after coating with a thin layer of vacuum grease to prevent water penetration in open pores. Helium pycnometry was first performed to measure open porosity.

Table 1
Initial conditions for NiTi (50.2 at.% Ni) billets 1–8 studied here. Samples A and B previously studied by Greiner et al. [14], with 51 at.% Ni, are also listed for comparison.

Sample	Backfill Ar pressure (atm)	HIP pressure (atm)	Porosity after HIP (%)
1	0.9	1800	0.09
2	1.4	1800	0.25
3	2.5	1800	0.43
4	5.3	1800	0.98
5	6.7	1800	1.34
6	11	1800	2.26
7	24	1800	3.92
8	33	1800	6.26
A [14]	2.1	1020	0.60
B [14]	4.5	1020	1.16

The total porosity of the foam f was calculated from the Archimedes sample density ρ as

$$f = \frac{\rho_{\mathrm{NiTi}} - \rho}{\rho_{\mathrm{NiTi}} - \rho_{\mathrm{Ar}}} \tag{1}$$

where ρ_{NiTi} is the density of NiTi, measured as 6.439 ± 0.001 g/cm^3 on a large sample densified from the same powders as the foams, but with no Ar backfill. For foamed samples where the Ar-filled pores have expanded, the Ar density, ρ_{Ar}, is small and can be neglected. For the densified billets, this assumption leads to sizeable errors: the density of the compressed Ar in the pores was calculated with the virial equation [18] based on the HIP pressure and temperature, as 0.496 g/cm^3 at room temperature (assuming no pore expansion during HIP depressurization at ambient temperature).

2.3. Ultrasonic measurement of Young's modulus

The Poison's ratio ν and Young's modulus E of the NiTi foams were calculated based on the measurement of sound longitudinal wave velocity V_{l} and shear wave velocity V_{s} from:

$$V_{\mathrm{s}} = \sqrt{\frac{E}{2\rho(1+\nu)}} \tag{2}$$

$$V_{\mathrm{l}} = \sqrt{\frac{E}{\rho}\frac{(1-\nu)}{(1+\nu)(1-2\nu)}} \tag{3}$$

where ρ is the foam density. Measurements were carried out in transmission on 5–10 mm long sample at a frequency of 5 MHz, using a high viscosity fluid (molasses) to couple the sample to the transducers. A digital oscilloscope recorded the time taken for the sound waves to be transmitted through the samples. Repeated measurements of time-of-flight through the samples showed less than ±0.01 μs difference. An additional systematic error was associated with the determination of the first rise in the signal on the receiving transducer, which was estimated to be <±0.1 μs. Even for the shortest time of flights (smallest samples with least porosity), the random error in velocity is only 0.4% and the largest systematic error possible is 4%, but is expected from measurement of calibration samples to be below 1%.

3. Results and discussion

3.1. Measurements of foaming kinetics

Fig. 1 shows that there is a linear relationship, as expected, between the Ar pressure within the can at ambient temperature before HIP densification and the billet initial porosity after HIP. Samples A and B by Greiner et al. [14] are included for comparison, but were densified at a lower pressure (103 MPa vs. 152 MPa) and thus show higher initial porosity for a given initial Ar pressure. Also, Ar pressures for samples 5–8 (for which Ar was solidified) were not

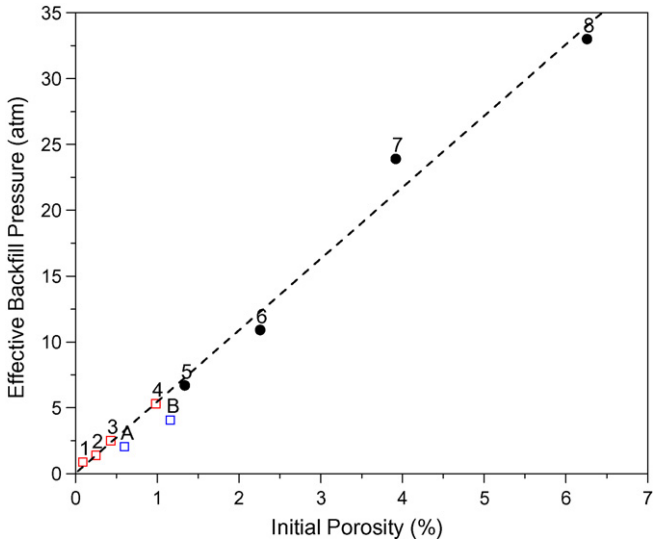

Fig. 1. Plot of backfill Ar pressure vs. initial as-HIP porosity. Solid symbols are for high-pressure samples (5–8) made with solid Ar, and open symbols are for low-pressure samples (1–4) produced with gaseous Ar. Samples A and B from Ref. [14] are also shown, and were densified under lower pressure, thus yielding higher initial porosity.

measured directly, but rather calculated from the metered gas, and have higher errors.

A first series of foaming tests was carried out on samples 5–8 at 1150 °C, close to the temperature of 1200 °C used by Greiner et al. [14] for samples A and B. Foaming for these four samples happened extremely rapidly: after only 5 min at temperature, porosity was nearly fully open and had reached values between 8% and 12%. When foamed for an additional 10 min at 1150 °C, sintering was observed to occur by an increase in closed porosity, as measured by helium pycnometry. A third anneal for 15 min closed by sintering a majority of the open porosity. This series of events sheds light on the unexpected foaming kinetics reported by Greiner et al. [14] for samples A and B and reproduced in Fig. 2: foaming rates decreased drastically after the foams reached 10–11% porosity, despite the fact that all porosity was found to be closed. The present experiments indicate that foams A and B, between two porosity measurements, lost their pressurized Ar by pores which opened to the surface and

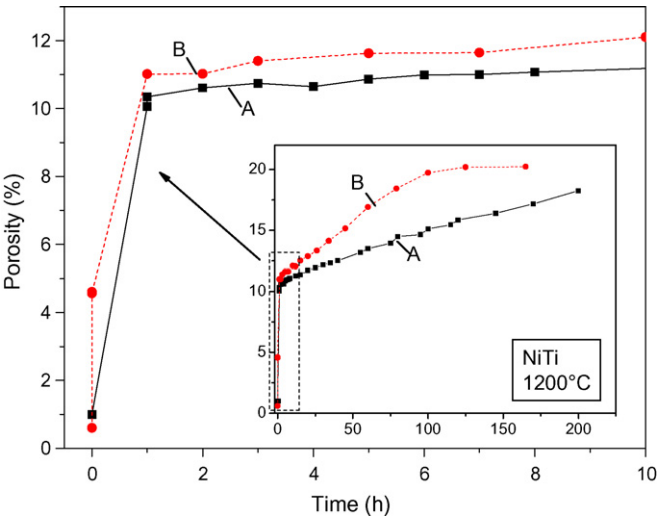

Fig. 2. Foaming curve for samples A and B foamed at 1200 °C by Greiner et al. showing a very fast initial rise followed by a very slow increase in porosity with time.

then rapidly reclosed by sintering. The subsequent very slow foaming occurred as a minority of small pressurized pores connected to the network of empty pores and re-pressurized them, albeit at a much smaller pressure. A schematic of the proposed process is given in Fig. 3

Foaming curves are shown in Fig. 4 for a second series of foaming experiments performed at 900 °C to study pore growth in more detail. The curves for samples 1–4 are not shown, because the foaming rate was very slow. Foaming for samples 5–7 was much slower than at 1200 °C, but remained very fast for sample 8 (f_o = 6.26%) which achieved a terminal porosity of 8.4% after 5 min. Fig. 4 shows that the initial foaming rate decreases with decreasing initial Ar pressure and the subsequent foaming rate decreases with foaming time, as expected qualitatively. Open porosity starts to appear when foams 5–7 reached ~11% total porosity, and increases continuously with foaming time. At 14% porosity, foaming rates are near zero, and the open porosity represents about half of the total porosity. A maximum porosity of 16% is reached for samples 7 and 6 after ~16 and 32 h of foaming, respectively, and sample 5 with the lowest initial Ar pressure, has not yet reached maximum porosity after 32 h.

3.2. Modeling of foaming kinetics

A simple analytical model has been used previously to describe the foaming kinetics of titanium containing pressurized, spherical pores within a creeping matrix, based on the creep expansion of a thick-walled spherical pressure vessel [19]:

$$\dot{f} = \frac{3A}{2}\frac{f(1-f)}{(1-f^{1/n})^n}\left(\frac{3}{2n}P_{\text{eff}}\right)^n \tag{4}$$

assuming that primary creep is negligible. In this equation, $\dot{f}$ is the rate change of porosity, f is the porosity, and P_{eff} is the effective Ar pressure. The parameters A and n come from the uniaxial creep equation:

$$\dot{\varepsilon} = A' \exp\left(\frac{-Q}{RT}\right)\sigma^n \tag{5}$$

where $\dot{\varepsilon}$ is the uniaxial creep rate, σ is the uniaxial stress, n is the stress exponent, Q is the activation energy, T is the temperature, R the gas constant, and A' is a material dependent constant. At constant temperature, the first two terms are combined as $A = A' \exp(-Q/RT)$. NiTi creep parameters reported in Ref. [17] were used. This simple analytical model was compared to finite-element calculations taking into account the overlapping stress fields of neighboring pores and found to give a very good approximation [19].

As compared to the original model [19], two modifications are implemented here in Eq. (4). First, Ar is not assumed to be an ideal gas, and the virial gas equation for the gas pressure P_{vir} is used:

$$P_{\text{vir}}V_m RT = 1 + \frac{B}{V_m} \tag{6}$$

where V_m is the molar volume of Ar and B is a fitting parameter determined by a Taylor expansion as $B(\text{m}^3) = -16 - 60(T_0/T - 1) - 10\ (T_0/T - 1)^2$ where T_0 = 293 K [18]. Second, an effective hydrostatic pressure P_s is considered to act on the pore due to the surface tension of solid NiTi, given by:

$$P_s = \frac{2\gamma}{r} \tag{7}$$

where γ is the surface energy of NiTi, and r is the pore radius. Then, the net Ar pressure P_o within the pores at the end of the HIP densification (with applied pressure P_{HIP}) is

$$P_o = P_{\text{HIP}} + P_s \tag{8}$$

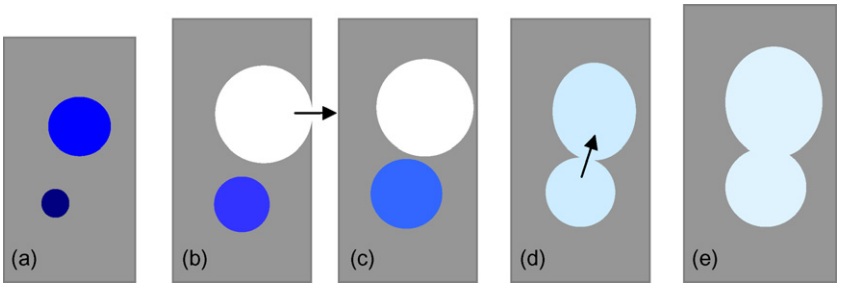

Fig. 3. Schematic diagram illustrating the mechanism of resintering and re-pressurization in NiTi showing (darkness of color represents pressure, white is vacuum): (a) two pressurized pores expand at different rates due to different size, (b) large pore connects to the surface losing its gas, (c) the large pore closes by sintering, (d) small pore continues to grow and connects to large pore and (e) merged pores with very low gas pressure grow slowly.

from which the initial pressure at the foaming temperature can be calculated using the virial equation. Similarly, the effective pore pressure during foaming, P_{eff}, is reduced by the surface tension as

$$P_{eff} = P_{vir} - P_s \quad (9)$$

The surface energy of solids is difficult to measure experimentally [20]. Even where data on surface tension in solids has been collected, it is most often pure metals [21,22]. It is much easier to experimentally measure the surface tension of materials in the liquid state, and there is a significant amount of data on pure metals and alloys in liquid form [18,23]. It is generally found that the solid surface tension is higher than the liquid surface tension [20]. The surface energy of pure liquid titanium at 1680 °C (slightly above the melting point of 1668 °C) was measured as 1.51 N/m, while the surface energy of solid titanium at 90 °C below the melting point was 1.70 N/m, an increase of ~13% [21]. The surface energy of NiTi could not be found in the literature and was estimated as follows. The surface energy in liquids generally scales with melting point, and based on published surface tension and melting point trends for pure metals [23], the extrapolated liquid surface tension of NiTi is estimated as 1.05 N/m. The surface energy for solid NiTi is then estimated to be 1.19 N/m, by using the same 13% increase in surface tension measured from liquid to solid titanium.

After introducing Eqs. (5)–(9) into the original foaming equation (Eq. (4)), the latter equation is solved iteratively and results are plotted in Fig. 5. Surface tension was found to make only a small difference in the calculations due to the large initial pressures (152 MPa) and the micron-sized pores (according to Eq. (7), the surface tension of a 1 μm radius pore is 2.4 MPa). Given the sizeable experimental errors and the many simplifications used in the model, the simulations results are in reasonable agreement with experimental data, which are plotted only up to the point where porosity opens to the surface and gas is lost. A possible explanation for the discrepancy between model and experiment for foams 6 and 7 is that the pore growth occurred too rapidly for pores to achieve a spherical shape by surface diffusion, and elongated pores grow more rapidly than spherical ones [19].

Table 2
Oxygen and carbon content of NiTi samples.

Sample	O (wt.%)	C (wt.%)
Prealloyed powder	0.1	0.003
NiTi Billet after HIP	0.075	0.015
NiTi foamed for 47 h[a]	0.1	0.029

[a] 400 cycles between 550 and 950 °C.

3.3. Foam microstructure and composition

As shown in Table 2, no significant oxygen contamination occurred during foaming. The carbon content is very low and may have increased slightly as a result of small remnants of the grease used in density measurements, which may have produced small amounts of TiC on the sample surface.

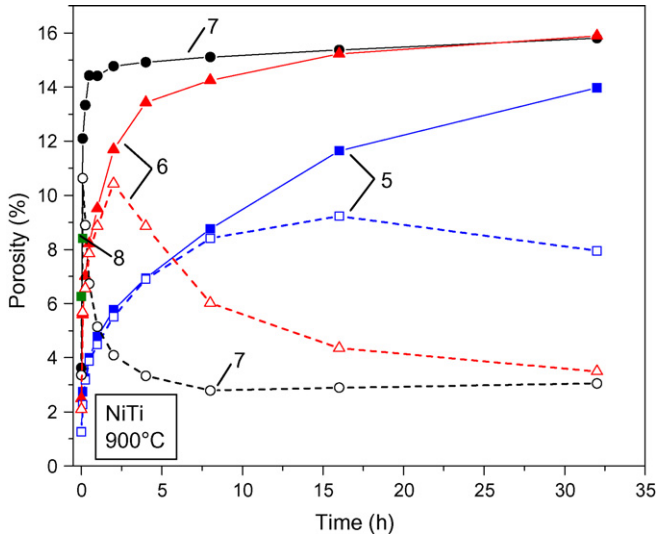

Fig. 4. Foaming curves for samples 5–7 foamed at 900 °C. Solid lines and solid symbols represent total porosity, dotted lines and open symbols represent closed porosity. The two green squares are for sample 8 with initial porosity of 6.29% and final porosity of 8.4% (mostly open) after 5 min of foaming.

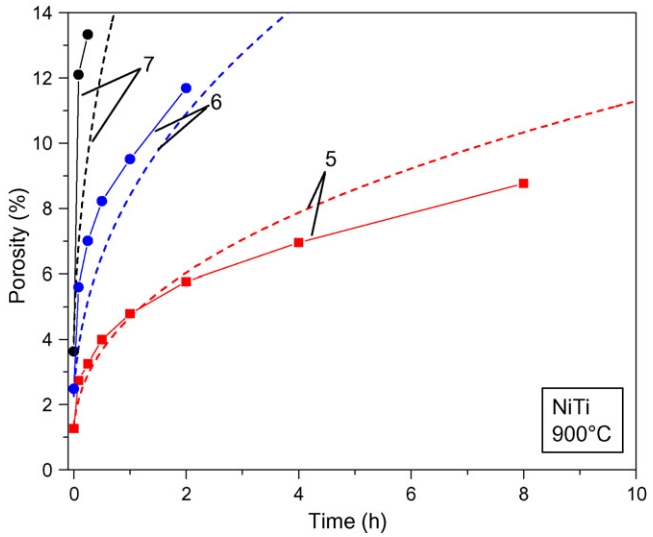

Fig. 5. Initial foaming curves (with fully closed porosity) for samples 5–7 foamed at 900 °C. Model predictions are shown with dotted lines.

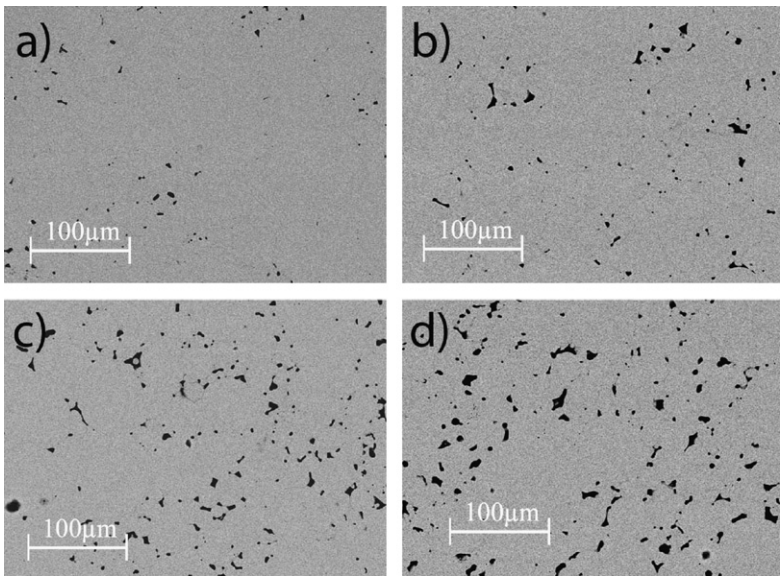

Fig. 6. Optical micrographs of as-densified NiTi billets showing increasing initial porosity f_o with increasing backfill pressure. (a) Sample 3, f_o = 0.43%, (b) sample 5, f_o = 1.34%, (c) sample 6, f_o = 2.26% (d) sample 7, f_o = 3.92%.

Micrographs of cross-sections of the HIP-densified billets (Fig. 6) illustrate that initial porosity increases with increasing backfill pressure, as expected from measurements reported in Fig. 1. As expected, pores are located at the boundaries of the former NiTi powders. The pore shape is not spherical, indicating that surface diffusion was not sufficient to spherodize the pores during the HIP process (4 h at 1066 °C).

Fig. 7(a) shows foam A with 17% porosity, which after 170 h at 1200 °C displays nearly spherical pores. By contrast, Fig. 7(b) shows foam 7 which reached 14% porosity after a much shorter time, 30 min, at the slightly lower foaming temperature of 1150 °C. The angular pores are interconnected to each other through crack-like channels. As for Fig. 7(a), the previous powder particles are easily recognizable. This is also the case for sample 5, foamed for 32 h at 900 °C, as shown in Fig. 8. As illustrated in this figure, most of the volume from the previous NiTi particles does not participate in the foaming, which is restricted to a network volume close to the prior powder surfaces.

This is unlike the situation observed in titanium foams [16], where an initially inhomogeneous distribution of small, high-pressure pores found at the prior powder particles grow into a much more homogenously distributed population of larger pores, by creep of the surrounding matrix. In NiTi, it appears that the prior particle boundaries are weakened, and thus fail with little creep deformation, forming rapidly a network of pores linked by

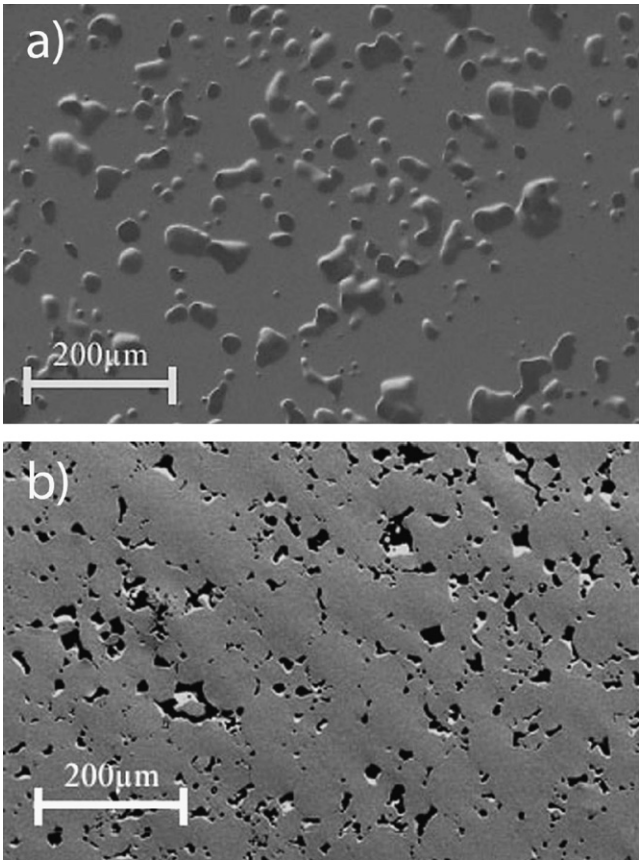

Fig. 7. SEM micrographs of NiTi after foaming (a) Sample A (f_o = 0.60%) foamed to porosity f = 17% after 170 h at 1200 °C. (b) Sample 7 (f_o = 3.92%) foamed to porosity f = 14% after 30 min at 1150 °C.

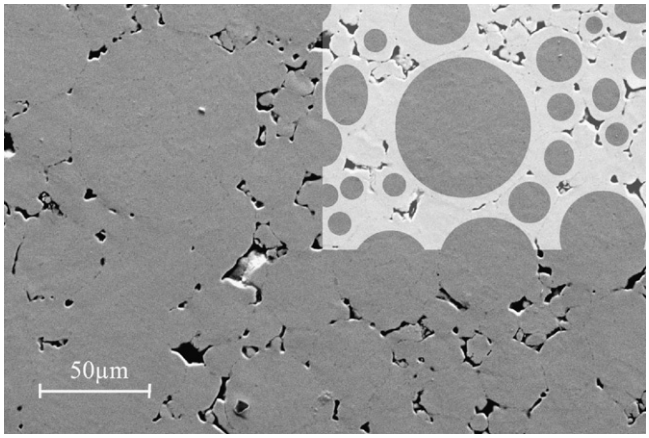

Fig. 8. SEM micrograph of sample 5 (f_o = 1.34%) foamed to porosity f = 14% after 32 h at 900 °C, showing network of elongated pores. Superimposed on top right of the micrograph are light-gray areas highlighting material that is deformed during foaming.

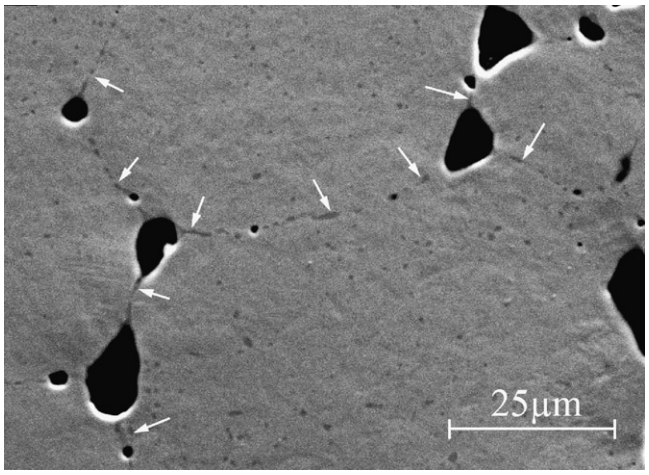

Fig. 9. SEM micrograph of sample 7 (f_o = 3.92%) foamed to porosity f = 14% after 30 h at 900 °C, showing the interface between previous powder particles decorated by darker oxide particles (arrows) and pores (black). The elongated pores are in the process of merging by fracture of the interface.

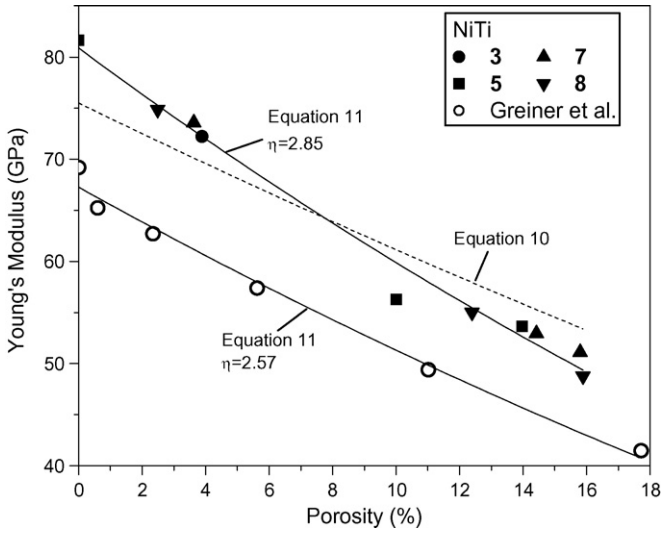

Fig. 10. Plot of Young's modulus measured ultrasonically vs. porosity, for NiTi foams from Greiner et al. [14] with 51 at.% Ni, and from the present study with 50.2 at.% Ni. Dotted and full lines show best-fit to Eqs. (10) and (11) with η values given in parentheses, respectively.

elongated crack-like channels. As shown in Fig. 9, the surface of the prior NiTi powders is decorated by numerous particles, forming a near-continuous film (visible as a darker band in Fig. 9). Due to their small size, composition of these particles could not be determined quantitatively by energy dispersive X-ray spectroscopy (EDS) which however indicated qualitatively an increase in titanium as compared to the matrix, in agreement with the presence of a titanium-rich oxide, probably formed during the powder solidification step. This oxide film is most likely responsible for the weakening of the interparticle regions leading to the early linkage of pores into a network, premature escape of gas, and termination of foaming in NiTi. By contrast, titanium dissolves its own oxide at elevated temperature, so oxide films on Ti powders disappear during the HIP process, and subsequent foaming can occur to much higher final porosities before pores link to each other and to the specimen surface [13,15,16,19].

3.4. Foam Young's modulus

The foam Young's modulus, as measured ultrasonically, is plotted as a function of foam porosity in Fig. 10. The data were fit to the Gibson–Ashby equation [24]:

$$\frac{E}{E_o} = \left(\frac{\rho}{\rho_o}\right)^2 \tag{10}$$

where E and E_o are the Young's moduli of the foam and the dense metal, ρ and ρ_o are the density of the foam and the dense metal. Data were also fitted to a modification of the above equation proposed by Wanner [25]:

$$\frac{E}{E_o} = \left(\frac{\rho}{\rho_o}\right)^n \tag{11}$$

where η is a fitting parameter increasing above 2 as pores become more elongated. A best fit is found for the present foams with η = 2.85, which is larger than 2 as expected given the non-spherical shape of the pores. Also plotted in Fig. 10 are ultrasonic moduli for the NiTi foams of A and B presented by Greiner et al. [14]. These foams are systematically less stiff than 1–8, which may be due to the difference in composition. The best-fit exponent is η = 2.57, close to the value for the present foams.

To reach a 15–25 GPa modulus for bone, the present foams would have to show a porosity of 35–45%. Such high porosity may not be needed since, as shown by Greiner et al. [14], the apparent stiffness of porous NiTi as measured from stress-strain curves, is significantly lower than the Young's modulus as measured ultrasonically. The explanation offered for the lower stiffness measured during compressive testing is the onset of reversible superelasticity during the linear, apparently elastic, loading and unloading of the foams, which occurs in small foam volumes with stress concentrations [14].

4. Conclusions

- Porous NiTi was created by entrapping Ar gas during powder densification and subsequently expanding the individual gas-filled pores at 900 or 1150 °C, in a creep expansion method previously demonstrated for titanium.
- Unlike titanium produced by this method, the porosity of NiTi does not exceed 16–20%, due to premature merging of pores into a network connecting to the sample surface where the gas is lost.
- Despite the non-spherical pore morphology, a simple gas expansion model can accurately predict the foaming behavior up to the onset of gas loss, and the foaming rates is strongly influenced by the initial Ar content of the densified billets. Surface tension plays a small role in the initial pore expansion, but is important at a later stage in reclosing open porosity.
- Porous NiTi exhibits Young moduli, as measured ultrasonically, which decrease with porosity in agreement with a simple analytical model, to 48 GPa for 16% porosity.
- Porous NiTi is an attractive material for biomedical implants, given its unique combination of desirable mechanical properties (low stiffness, high strength and superelastic/shape-memory strain), its biocompatibility and its open porosity allowing bone ingrowth.

Acknowledgments

This research was supported by U.S. National Science Foundation through Grant DMR-0505772. S.M.O. also acknowledges the U.S. Department of Defense for a NDSEG Fellowship. The authors thank Dr. Jan Frenzel from the Ruhr-Universität Bochum (Germany) for performing chemical analysis of the NiTi samples.

References

[1] S. Prokoshkin, V. Pushin, E. Ryklina, I. Khmeleyskaya, Phys. Metal Metall. 97 (2004) 56–96.

[2] L. Ponsonnet, D. Treheux, M. Lissac, N. Jaffrezic, B. Grosgogeat, Int. J. Appl. Electromag. Mech. 23 (2006) 147–151.
[3] K. Otsuka, X. Ren, Prog. Mater. Sci. 50 (2005) 511–678.
[4] A. Bansiddhi, T.D. Sargeant, S.I. Stupp, D.C. Dunand, Acta Biomater. 4 (2008) 773–782.
[5] Y. Zhang, D. Li, X. Zhang, Scripta Mater. 57 (2007) 1020–1023.
[6] S. Wu, C. Chung, X. Liu, C. Chu, Y. Chan, K. Yeung, W. Lu, K. Cheung, K. Luk, Acta Mater. 55 (2007) 3437–3451.
[7] D.C. Lagoudas, E.L. Vandygriff, J. Intel. Mater. Systems Struct. 13 (2002) 837–850.
[8] H. Jiang, L. Rong, Mater. Sci. Eng. A 438 (2006) 883–886.
[9] A. Bansiddhi, D.C. Dunand, Intermetallics 15 (2007) 1612–1622.
[10] A. Bansiddhi, D.C. Dunand, Acta Biomater. 4 (2008) 1996–2007.
[11] B. Bertheville, Biomaterials 27 (2006) 1246–1250.
[12] D.S. Grummon, J.A. Shaw, A. Gremillet, Appl. Phys. Lett. 82 (2003) 2727–2729.
[13] M.W. Kearns, P.A. Blenkinsop, A.C. Barber, T.W. Farthing, Int. J. Powder Metall. 24 (1988) 59–64.
[14] C. Greiner, S.M. Oppenheimer, D.C. Dunand, Acta Biomater. 1 (2005) 705–716.
[15] N.G.D. Murray, D.C. Dunand, J. Mater. Res. 21 (2006) 1175–1188.
[16] N.G.D. Murray, D.C. Dunand, Compos. Sci. Technol. 63 (2003) 2311–2316.
[17] S.M. Oppenheimer, A.R. Yung, D.C. Dunand, Scripta Mater. 57 (2007) 377–380.
[18] Handbook of Chemistry and Physics, 81st ed., CRC, 2000/2001.
[19] N.G.D. Murray, D.C. Dunand, Acta Mater. 52 (2004) 2279–2291.
[20] Bikerman, Surface Chemistry, Academic Press Inc., 1958.
[21] H. Jones, Metal Sci. J. 5 (15) (1971) 15–18.
[22] D.A. Porter, K.E. Easterling, Phase Transformations in Metals and Alloys, Nelson Thornes, 1981.
[23] B.J. Keene, Int. Mater. Rev. 38 (4) (1993) 157–191.
[24] L.J. Gibson, M.F. Ashby, Cellular Solids, Cambridge University Press, Cambridge, 1997.
[25] A. Wanner, Mater. Sci. Eng. 248A (1998) 35–43.
[26] A. Bansiddhi, D.C. Dunand, J. Mater. Res. 24 (6) (2009) 2107–2117.